SEVA: An externally driven framework for reproducing COVID-19 mortality waves without transmission feedback

Kim Varming
Independent researcher
Aalborg, Denmark
e-mail: varming.kim@gmail.com

Keywords: epidemic modelling; depletion dynamics; logistic hazard; COVID-19; mortality

Abstract

Understanding the dynamical mechanisms underlying epidemic wave formation remains a central problem in mathematical epidemiology. Population-level epidemic waves are commonly interpreted as emergent consequences of nonlinear transmission feedback between susceptible and infectious individuals. However, epidemic time series from different regions often display markedly different waveform regimes, ranging from sharply peaked epidemics with rapid post-peak decline to more prolonged plateau-like dynamics.

Here we propose the SEVA (Seasonal/Environmental Viral Activity) framework as a parsimonious alternative dynamical interpretation of epidemic wave formation. In this formulation, epidemic waveforms arise from depletion of a finite vulnerable population under a temporally structured viral activity field. The activity function is represented by a monotonic logistic hazard describing the temporal evolution of viral activity. With activation timing and steepness held constant across regions, daily incidence emerges as the product of activity intensity and the remaining vulnerable population.

The framework is applied to first-wave COVID-19 hospitalization and mortality data from selected European countries and U.S. states during spring 2020. With fixed activation parameters and region-specific activity intensity, the model provides a simple dynamical explanation for diverse epidemic waveform regimes—including sharply peaked waves and plateau-like dynamics—without modification of the underlying dynamical structure.

When epidemic trajectories are expressed in normalized form, curves from regions with very different mortality burdens display closely similar temporal structures. Within the SEVA formulation, this behaviour arises naturally from the interaction between a common temporal activation profile and regionally varying activity intensity. In this perspective, sharply peaked epidemics and plateau-like trajectories represent different dynamical regimes of the same activity-driven depletion process.

1. Introduction

Mathematical models play a central role in describing the dynamical behaviour of infectious disease epidemics at the population level. In many classical formulations, epidemic growth and decline arise from interaction-driven feedback between susceptible and infectious individuals. In such SIR-type frameworks, population-level epidemic waveforms emerge from nonlinear transmission processes coupled to depletion of susceptible individuals (Kermack and McKendrick, 1927; Anderson and May, 1991; Keeling and Rohani, 2008).

These formulations have been widely applied to respiratory virus epidemics, where epidemic peaks are typically interpreted as the consequence of transmission amplification followed by depletion of susceptible individuals. At the same time, seasonal and environmental modulation of respiratory viruses has long been recognised (Dowell, 2001; Shaman and Kohn, 2009; Tamerius et al., 2011). Environmental stability of viral particles, variation in host susceptibility, immune landscape dynamics, and behavioural synchronisation may all contribute to temporally structured exposure at the population level.

Comparative analyses of respiratory epidemics have revealed substantial variation in epidemic waveform dynamics across regions. During the first COVID-19 wave, some regions exhibited sharply peaked epidemic curves with rapid post-peak decline, whereas others displayed more prolonged plateau-like dynamics over similar time intervals. Such differences in waveform structure suggest that the mechanisms governing epidemic timing and decline may vary across settings and are not necessarily explained by transmission amplification alone.

This observation raises the question of whether the characteristic asymmetric rise–peak–decline structure observed in many respiratory epidemics can arise from temporally structured exposure processes rather than from transmission feedback alone.

In this study, we examine a minimal activity-driven depletion framework in which epidemic waveforms emerge from the interaction between a time-varying external activity function and a finite vulnerable pool. Rather than modelling infection incidence directly, the model describes observed endpoints—hospitalization and mortality—as arising from depletion under a structured hazard function.

The objective of the present study is to evaluate whether this minimal dynamical formulation is sufficient to reproduce the characteristic temporal structure of first-wave COVID-19 hospitalization and mortality data across diverse regions. By focusing on waveform dynamics at the level of observable endpoints, the analysis addresses the structural requirements necessary to generate large-scale epidemic patterns under externally modulated activity.

2. Model and methods

2.1 Model structure

We model epidemic waveforms at the level of observed endpoints (mortality and hospitalizations) using a parsimonious depletion framework.

- $V(t)$ denotes the vulnerable pool (proportion of the population) that can contribute to the endpoint during the analysed wave,
- $C(t)$ denotes the cumulative endpoint count (deaths or hospitalizations, expressed as proportion of the population).

The model is driven by a time-varying activity function $A(t)$ (day^{-1}), interpreted as an aggregated per-capita hazard acting on the vulnerable pool.

The structural components of the SEVA framework are illustrated schematically in Figure 1.

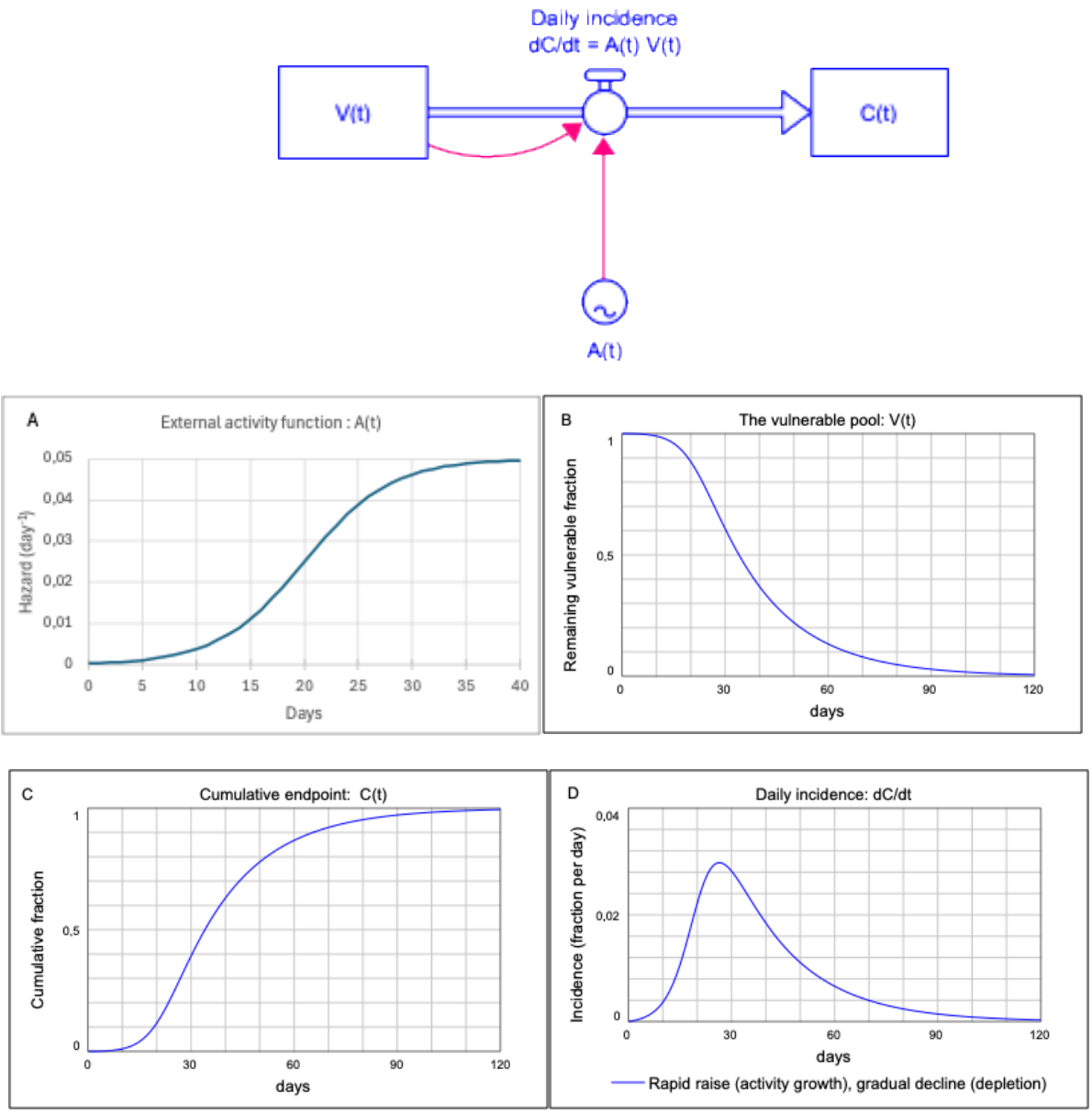

Figure 1. Structural dynamics of the SEVA depletion framework.
Top: Conceptual structure of the model. A time-varying external activity function *A(t)* acts on a finite vulnerable pool *V(t)*, generating cumulative endpoints *C(t)* with daily incidence $dC/dt = A(t)V(t)$.
(A) External activity function *A(t)*.
(B) Depletion of the vulnerable pool *V(t)*.
(C) Cumulative endpoint *C(t)*.
(D) Resulting daily incidence *dC/dt*. The asymmetric rise–peak–decline waveform arises from the interaction between increasing activity and depletion of the vulnerable population.

2.2 Activity-driven hazard function

The activity driver is defined as:

$$A(t) = p_max / (1 + exp[-k(t - t_0)])$$

where p_max (day^{-1}) is the maximal hazard, k (day^{-1}) controls activation steepness, and t_0 (days) determines the temporal midpoint of activation.

The logistic function was chosen as a minimal smooth activation profile that provides independent control of amplitude (p_max), timing (t_0), and steepness (k).

It yields bounded growth, ensures differentiability, and avoids discontinuities that would introduce artificial kinks in the hazard profile. These properties allow transparent separation of intensity and time-scale effects in the resulting depletion dynamics.

Although asymptotic in time, for the parameter values used (k = 0.25, t_0 = 20), activity increases from approximately 0.7% to 99.3% of its maximum between day 0 and day 40, effectively corresponding to a finite activation window in the simulations.

2.3 Dynamical equations

Endpoint accumulation is described by the system:

$dV/dt = -A(t)V(t)$,

$dC/dt = A(t)V(t)$,

with initial conditions $V(0) = V_0$ and $C(0) = 0$.

The system conserves the endpoint-relevant population:

$V(t) + C(t) = V_0$

Expressed in fractional form, defining

$F(t) = C(t)/V_0$,

the system can be written as

$dF/dt = A(t)\ (1-F)$

This formulation highlights that the daily incidence arises from the interaction between the activity driver and the remaining undepleted fraction of the vulnerable population.

Because activity increases monotonically while the vulnerable pool is simultaneously depleted, the rising phase of the epidemic is primarily driven by activity growth, whereas the declining phase is governed by depletion of the vulnerable population. This interaction naturally produces asymmetric epidemic waveforms.

2.4 Parameter exploration

We examined the influence of the parameters *p_max*, t_0, and *k* on the temporal waveform properties of the daily incidence *dC/dt*. (Fig. 2)

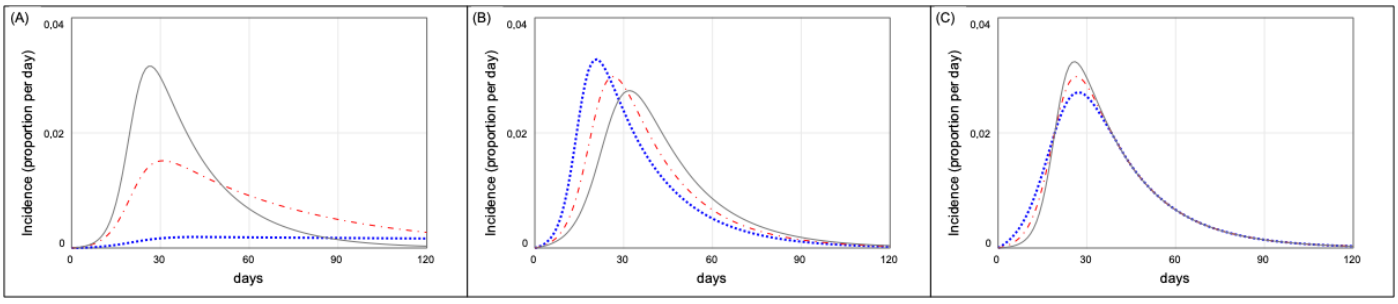

Figure 2. Parameter sensitivity of the activity-driven depletion model.
(A) *p_max* varied (0.002, 0.02, 0.05) with fixed $t_0 = 20$ and $k = 0.25$.
(B) t_0 varied (15, 20, 25) with fixed *p_max* = 0.05 and $k = 0.25$.

(C) k varied (0.20, 0.25, 0.30) with fixed p_max = 0.05 and t_0 = 20.
Dotted, dashed, and solid lines represent increasing parameter values.

Parameter sensitivity analysis demonstrates distinct structural roles of the three parameters:

• p_max primarily controls peak amplitude and the rate of post-peak depletion, thereby influencing both the height of the peak and the duration of the declining phase.

• t_0 shifts the waveform along the time axis with minimal effect on its intrinsic shape.

• k modulates the acceleration phase by controlling the steepness of activation.

Together these parameter roles illustrate the core SEVA mechanism: epidemic waveforms arise from the interaction between a rising activity function and depletion of the vulnerable pool.

This parameter dependence reflects the underlying dynamical balance between activity growth and depletion of the vulnerable population. Within the SEVA formulation the epidemic turning point occurs when the growth of the activity function is balanced by depletion of the vulnerable pool.

2.5 Interpretation of the vulnerable pool

The vulnerable pool $V(t)$ is endpoint-specific. For mortality, $V(t)$ represents the effective subset of the population capable of contributing to deaths within the analysed wave. For hospitalization, it represents the corresponding subset capable of contributing to hospital admissions.

The size of this pool implicitly captures heterogeneity in age structure, comorbidity burden, and pre-existing protection within a given region and time window. The proportionality assumption is local to the analysed wave and region.

This formulation avoids explicit modeling of infection incidence. Because infection incidence is not directly observed, parameters such as the infection fatality ratio (IFR) are not independently identifiable from endpoint data alone (Brookmeyer and Gail, 1988). The SEVA framework therefore operates at the level of observable endpoints rather than inferred infection counts.

2.6 Data sources

2.6.1 Mortality data – Europe

Observed COVID-19 mortality data for European countries were obtained from the European Centre for Disease Prevention and Control (ECDC) COVID-19 surveillance database (European Centre for Disease Prevention and Control, 2020). Daily death counts were expressed per 100,000 population and smoothed using a 7-day moving average prior to analysis.

2.6.2 Mortality data – United States

State-level mortality data for the United States were obtained from the COVID Tracking Project (The COVID Tracking Project, 2021), which compiled harmonized daily death counts reported by official state and territorial health authorities. Daily mortality rates per 100,000 population were computed and smoothed using a 7-day moving average prior to analysis.

2.6.3 Reporting variability and smoothing

Daily mortality reporting exhibits substantial short-term variability due to reporting delays, weekend effects, and administrative batching. The 7-day moving average therefore provides a more stable representation of the underlying epidemic waveform used for model comparison (Fig. 3).

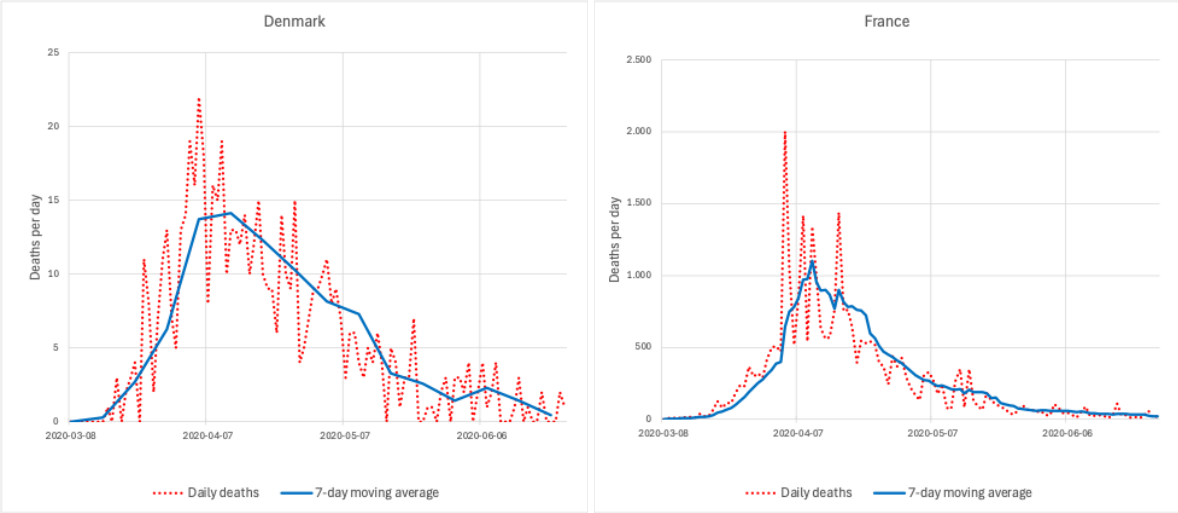

Figure 3. Reporting variability in daily mortality data.
The figure shows daily reported COVID-19 deaths in Denmark and France from the ECDC surveillance dataset together with the corresponding 7-day moving average calculated in this study.

2.6.4 Hospitalization data

Hospital admission data were obtained from *Our World in Data* (Mathieu et al., 2020), which aggregates officially reported national datasets. Weekly hospital admissions per million population were converted by Our World in Data to daily values using linear interpolation between weekly reporting points. No additional smoothing was applied to these series prior to temporal alignment and model comparison. Because the underlying data represent weekly aggregates, the interpolated daily series already exhibit reduced short-term variability relative to raw daily reporting data.

All analyses focused on the first epidemic wave during spring 2020, corresponding approximately to the first four months following epidemic onset in each region. Quantitative goodness-of-fit metrics were computed over a standardized 100-day window within this period to ensure comparability across regions.

2.7 Calibration procedure

Calibration was performed in two sequential steps to separate endpoint magnitude from waveform dynamics.

Default activation parameters

Unless otherwise specified, $t_0 = 20$ days and $k = 0.25$ day^{-1} were used as default activation parameters. Sensitivity analysis indicated that waveform morphology was robust to moderate variation in t_0 and k, and default values were therefore retained to reduce parameter dimensionality.

Step 1: Endpoint magnitude

For each region and endpoint, the initial vulnerable pool $V(0)$ was estimated by matching cumulative model output to the observed cumulative endpoint total over the analysis interval. This step ensures that differences in overall endpoint magnitude are accounted for independently of temporal waveform structure.

Step 2: Waveform shape

With endpoint magnitude fixed, the activity intensity parameter p_max was adjusted to reproduce the temporal morphology of the observed daily endpoint curve, including peak height, asymmetry, and rate of decline.

Parameter estimation prioritised structural correspondence of waveform features rather than formal optimisation of residual error.

2.8 Temporal alignment

Because the onset timing of underlying infections is not directly observable, model–data comparisons were performed using temporal alignment of waveform structure.

For each region and endpoint, a single constant time shift was applied to align simulated and observed curves. The shift was determined by matching peak timing and overall waveform morphology in the daily endpoint series.

2.9 Goodness-of-fit metrics

Model fit was quantified using root mean square error (RMSE), coefficient of determination (R^2), and Pearson correlation coefficient (r), computed on temporally aligned daily endpoint series.

For each region and endpoint, the analysis window was defined as a fixed 100-day interval beginning on the date of the first recorded death. This standardized window was used to ensure comparability of waveform dynamics across regions.

All metrics were calculated on daily incidence rather than cumulative counts, as cumulative series are monotonic and can artificially inflate goodness-of-fit statistics through integration of small residual errors.

2.10 Normalization

For cross-regional comparison of waveform morphology independent of absolute endpoint magnitude, we constructed a dimensionless representation by scaling cumulative endpoints to unity at the end of the analysis window T.

$$\hat{C}(t) = C(t) / C(T)$$

where T denotes the final day of the analysis window.

The corresponding daily incidence was expressed as a fraction of total cumulative endpoints:

$$d\hat{C}/dt = dC/dt/C(T)$$

This normalization removes differences in absolute endpoint magnitude and allows direct comparison of intrinsic epidemic waveform dynamics across regions.

To illustrate the behaviour of the normalized representation under the SEVA formulation, Fig. 4 shows simulated normalized trajectories for a range of activity intensities p_max while keeping the activation parameters k and t_0 constant. Under this representation, differences in absolute epidemic size are removed and the remaining variation reflects differences in activity intensity and the resulting depletion dynamics.

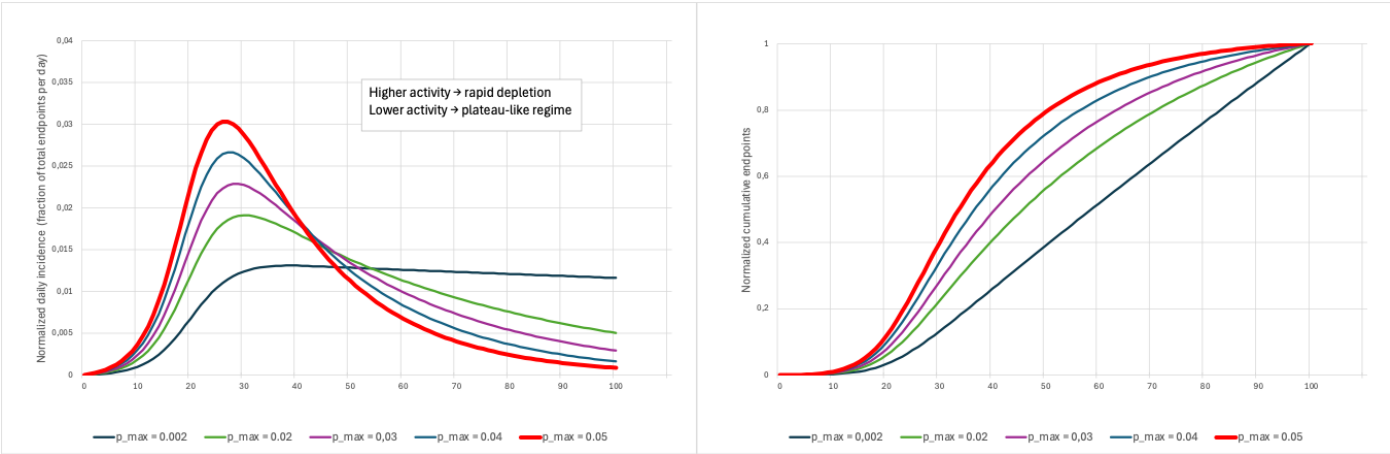

Figure 4. Theoretical normalized epidemic trajectories under the SEVA framework.
Left: normalized daily incidence *(dC/dt)/C(T)*.
Right: normalized cumulative endpoint *C(t)/C(T)*.
Curves are shown for varying values of the activity intensity parameter *p_max* while keeping *k* and t_0 constant. The normalized representation removes differences in absolute epidemic size and illustrates the waveform regimes expected under the SEVA formulation.

For the reference parameter setting used in this study ($k = 0.25$, $t_0 = 20$), the simulated turning point in the high-activity regime occurs at approximately day 28. This reference behaviour provides a useful baseline for comparison with the normalized empirical curves presented in the Results section.

2.11 Simulation environment

All model simulations were implemented using Stella Architect (Isee Systems, Lebanon, New Hampshire, USA). The software was used to define the stock–flow structure, parameterize model equations, and generate time-series outputs for comparison with empirical endpoint data.

Simulations were performed using explicit Euler integration with a daily time step ($\Delta t = 1$ day). Given the characteristic time scale of activation ($k \approx 0.25$ day^{-1}), this discretization is sufficient to ensure numerical stability and negligible integration error relative to waveform morphology.

In the graphical implementation, the activation window was specified over a 40-day interval. This corresponds to the analytical logistic formulation with $k = 0.25$ day^{-1} and $t_0 = 20$ days, for which activity increases from approximately 0.7% to 99.3% of its maximum between day 0 and day 40.

3. Results

We first examine the intrinsic structual behaviour of the model before applying it to empirical data.

3.1 Structural behaviour of the activity-driven depletion model

The SEVA framework describes endpoint dynamics through depletion of a finite vulnerable pool *V(t)* under a time-varying activity hazard *A(t)*, with daily incidence

$$dC/dt = A(t)\ V(t).$$

Although *A(t)* increases monotonically toward a plateau, the product *A(t)V(t)* generates a unimodal daily waveform. The initial rise phase is governed primarily by increasing activity, whereas the post-peak decline arises from progressive depletion of the vulnerable pool. The peak occurs when the growth of the activity function is balanced by depletion of the vulnerable pool.

his mechanism produces an intrinsically asymmetric rise–peak–decline structure without requiring explicit delay distributions or multi-stage progression dynamics. The cumulative endpoint *C(t)* follows a sigmoidal trajectory approaching an asymptote as *V(t)* decreases. Waveform asymmetry therefore arises directly from the structural interaction between monotonic activation and depletion.

3.2 Mortality dynamics during the first epidemic wave in Europe

Figure 5 shows observed and simulated daily COVID-19 mortality (per 100,000 population) for the same European countries during the first epidemic wave.

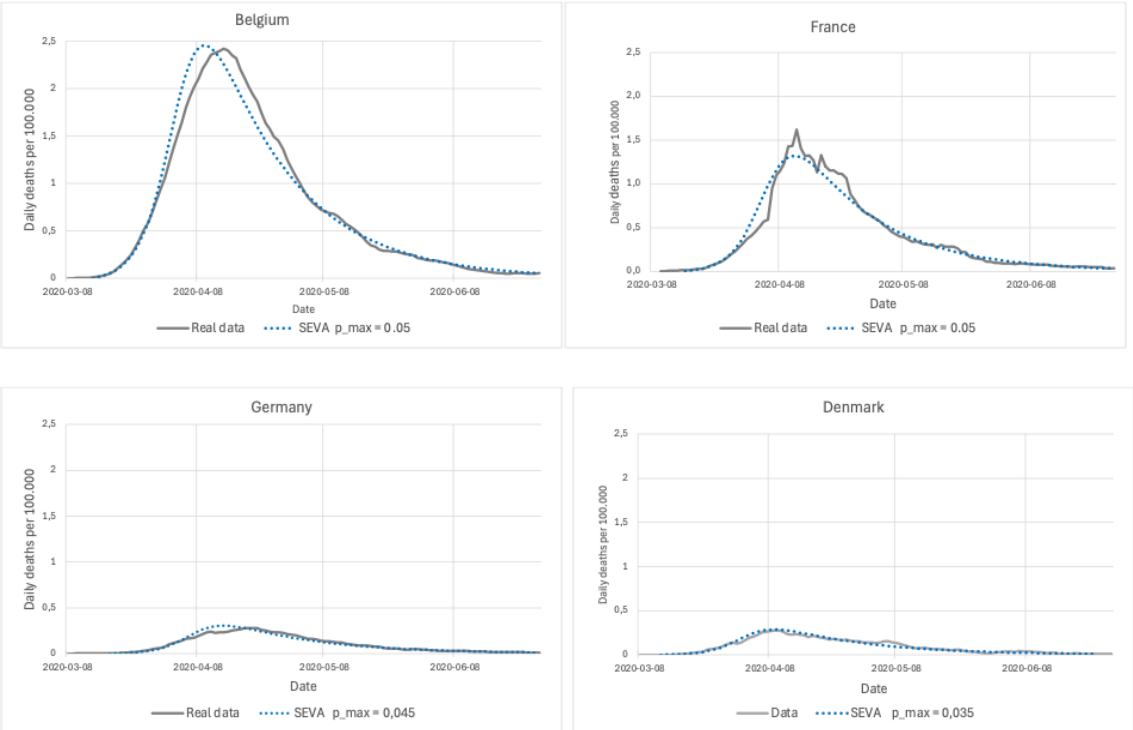

Figure 5. Mortality incidence during the first COVID-19 wave in selected European countries. Observed daily COVID-19 mortality (per 100,000 population) is shown together with SEVA model outputs using fixed activation parameters ($t_0 = 20$, $k = 0.25$) and country-specific *p_max*. The model captures the asymmetric waveform structure across countries without structural modification.

Mortality time series display waveform morphology similar to the hospitalization dynamics, including a rapid rise, a distinct peak, and prolonged decline. With the same activation parameters ($t_0 = 20$, $k = 0.25$), the model reproduces the temporal structure of the mortality curves through variation in *p_max* alone.

As in hospitalization analyses, inter-country differences in peak sharpness and decline rate correspond to differences in activity intensity, while cumulative mortality levels are determined independently through endpoint-specific scaling. Similar waveform reproduction is observed across 12 additional European countries (Fig. S1), supporting the generality of the structural formulation.

3.3 First-wave hospitalization dynamics in selected European countries

Figure 6 presents observed and simulated daily COVID-19 hospital admissions (per 100,000 population) for selected European countries during the first epidemic wave in spring 2020.

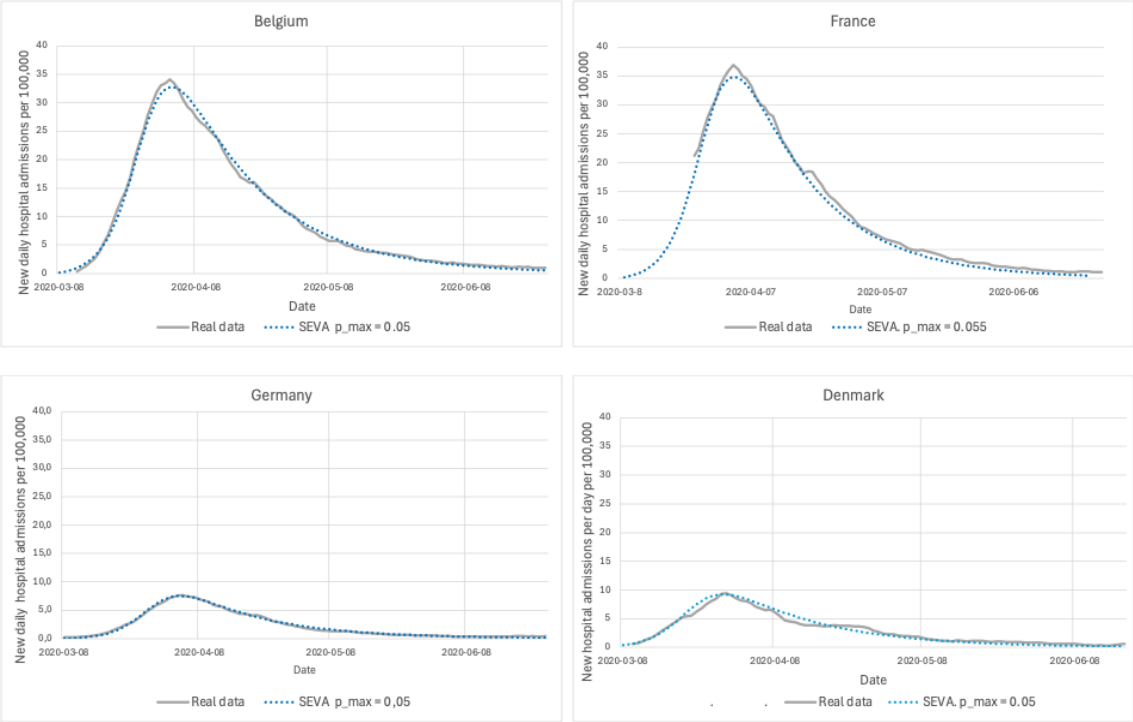

Figure 6. Hospitalization incidence during the first COVID-19 wave in selected European countries. Observed daily hospital admissions (per 100,000 population) are shown together with SEVA model outputs using fixed activation parameters ($t_0 = 20$, $k = 0.25$) and country-specific *p_max.* The model reproduces the asymmetric waveform structure across countries without structural modification.

Using fixed activation parameters ($t_0 = 20$, $k = 0.25$) variation in the activity intensity parameter p_max alone reproduces the observed hospitalization waveforms across countries.

All countries exhibit asymmetric waveforms characterised by rapid early growth followed by more gradual decline.

Differences in peak height and decay rate correspond to differences in activity intensity, whereas total cumulative admissions are matched independently through scaling of the initial vulnerable pool. No modification of the underlying dynamical equations was required across countries.

3.4 Regional mortality dynamics in the United States

Figure 7 contrasts mortality dynamics between selected northern and southern U.S. states during the first epidemic wave. The analysis window was restricted to the initial epidemic period (through late June 2020) in order to isolate first-wave dynamics prior to subsequent summer increases.

Panel A: Northern U.S. states	Panel B: Southern U.S. states
Higher activity intensity	Lower activity intensity
p_max ≈ 0.04–0.05	*p_max* ≈ 0.002
→ rapid depletion	→ incomplete depletion
→ clear turning point	→ plateau-like dynamics

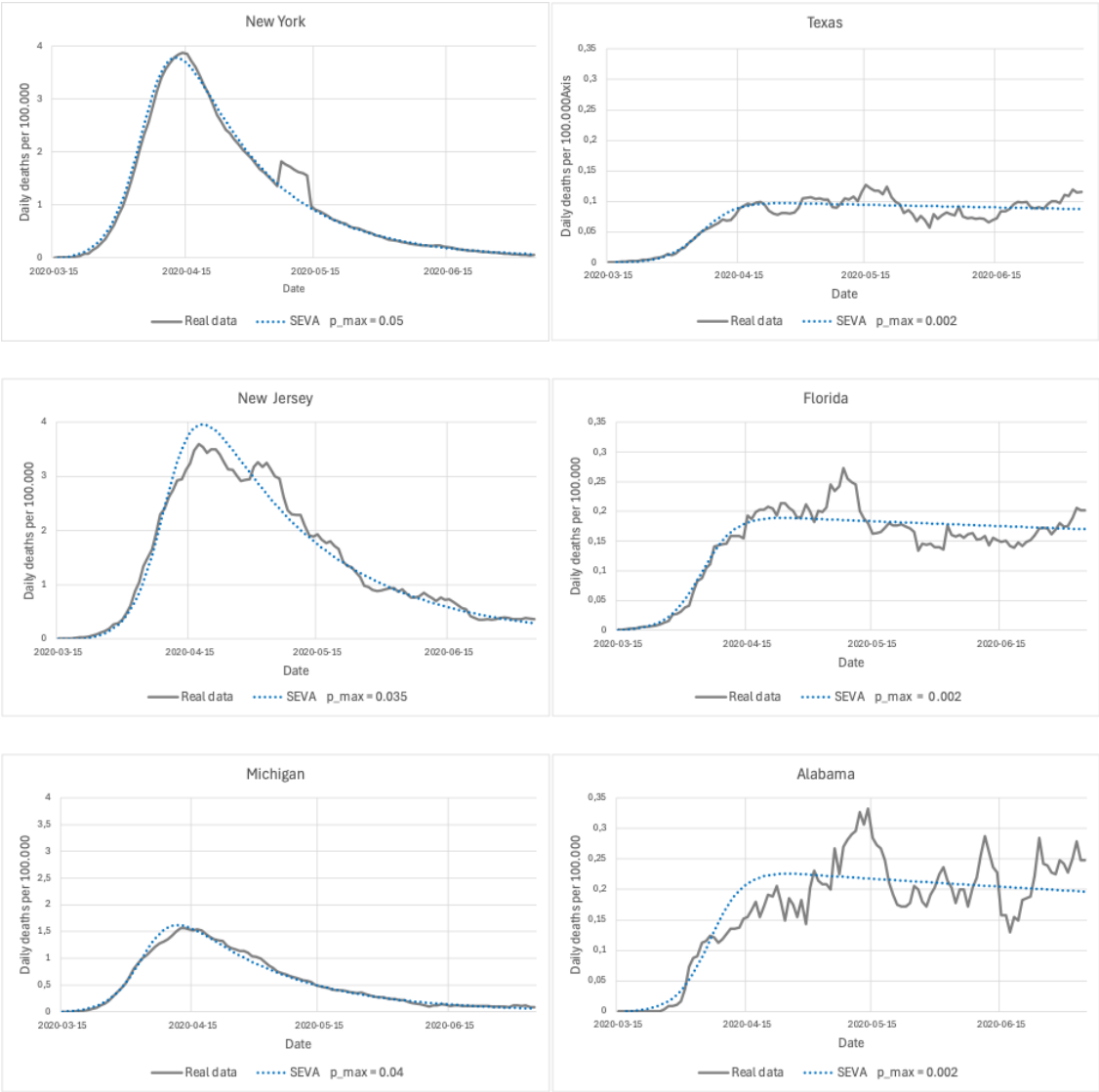

Figure 7. Regional contrast in COVID-19 mortality dynamics between northern and southern U.S. states.
Observed daily COVID-19 mortality (per 100,000 population) is shown together with SEVA model outputs using fixed activation parameters ($t_0 = 20$, $k = 0.25$) and state-specific activity intensity *p_max*.
Northern states exhibit sharply peaked epidemic curves with clear turning points, consistent with rapid depletion of the vulnerable pool under higher activity intensity.
Southern states display broader or plateau-like dynamics consistent with incomplete depletion under lower activity intensity.
Note: y-axis scales differ between panels.

The contrast between northern and southern states illustrates two distinct dynamical regimes within the SEVA framework.

With activation timing and steepness held constant, both waveform types are reproduced through variation in activity intensity and endpoint scaling alone.

In northern states, the turning point occurs within the analysis window and corresponds to substantial depletion of the endpoint-specific vulnerable pool. In southern states, the absence of sustained decline within the window is consistent with incomplete depletion under lower activity intensity.

Together, these observations indicate that diverse epidemic waveform morphologies across regions and endpoints can be reproduced within the same activity-driven depletion framework. The remaining analyses therefore focus on normalized waveform dynamics to examine structural similarities independent of absolute endpoint magnitude.

3.6 Normalized waveform regimes

Using the dimensionless representation defined in Section 2.10 removes cross-regional differences in absolute endpoint magnitude and allows direct comparison of intrinsic epidemic waveform dynamics.

3.6.1 Turning-point regime

Figure 8 shows normalized cumulative and daily mortality curves for regions in which a turning point occurs within the analysis window.

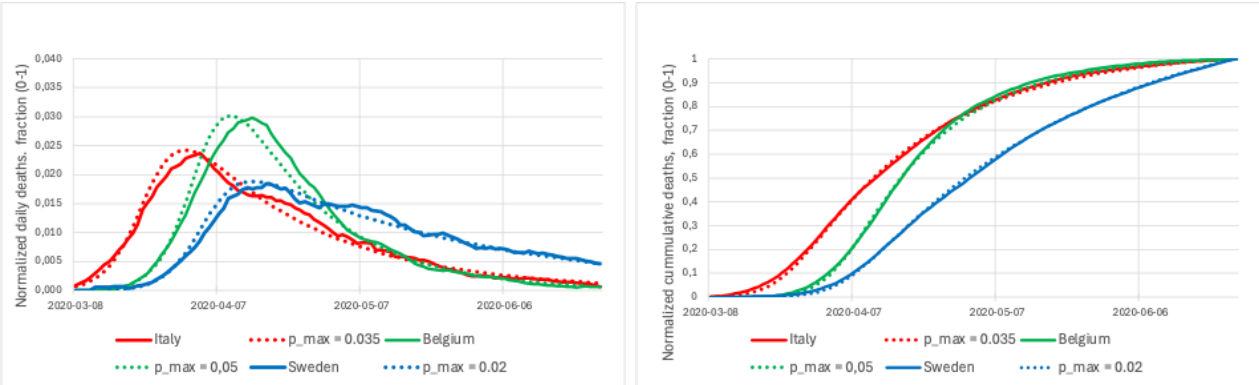

Figure 8. Normalized mortality dynamics in regions exhibiting a turning point within the analysis window.
Cumulative mortality was normalized to unity at the end of the first-wave analysis window. Daily mortality is expressed as a fraction of total cumulative mortality. Regions shown exhibit a clear turning point followed by sustained decline. Solid lines represent observed data; dotted lines represent SEVA model outputs with fixed activation parameters ($t_0 = 20$, $k = 0.25$) and region-specific *p_max*. Under this dimensionless representation, waveform morphology is directly comparable independent of absolute mortality magnitude.

Under normalization, daily incidence exhibits a clearly unimodal profile characterised by rapid rise, distinct peak, and sustained post-peak decline. The cumulative curves display pronounced sigmoidal curvature consistent with substantial depletion during the observed interval.

Within the SEVA framework, this behaviour arises under higher activity intensity. Variation in *p_max* modifies peak sharpness and timing while preserving the underlying structural form.

3.6.2 Activation-dominated regime

Figure 9 presents normalized curves for regions in which no pronounced turning point occurs within the analysis window.

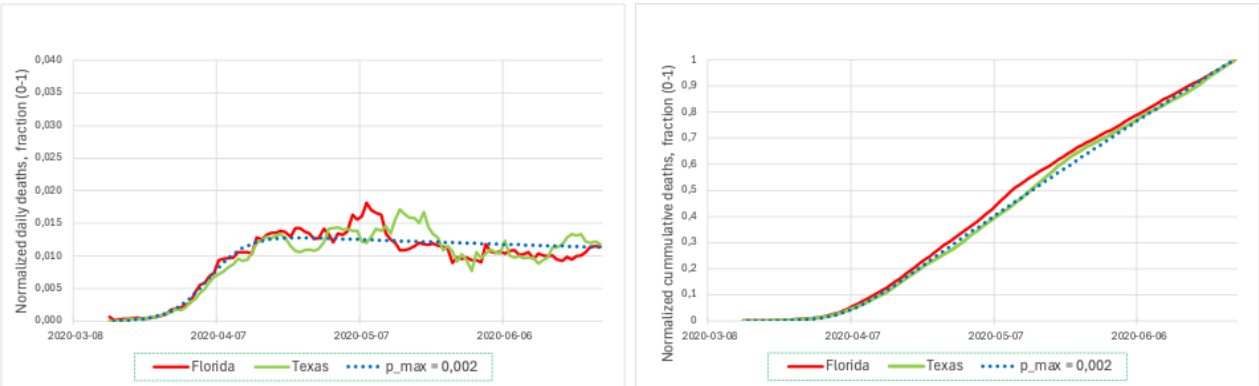

Figure 9. Normalized mortality dynamics in regions without a turning point within the analysis window.

Cumulative mortality was normalized to unity at the end of the first-wave analysis window. Daily mortality is expressed as a fraction of total cumulative mortality. Regions shown do not exhibit a pronounced turning point within the window. Solid lines represent observed data; dotted lines represent SEVA model outputs with fixed activation parameters ($t_0 = 20$, $k = 0.25$) and region-specific p_max. Under this dimensionless representation, waveform morphology is directly comparable independent of absolute mortality magnitude.

In these cases, normalized daily incidence rises and remains elevated without sustained decline over the observation period. The cumulative curves exhibit near-linear growth across much of the interval, indicating limited depletion relative to ongoing activation.

The depletion fraction is defined as

$C(T)/V_0$

i.e., the proportion of the endpoint-specific vulnerable pool depleted by time T.

For $p_max = 0.002$ with fixed $t_0 = 20$ and $k = 0.25$, the model yields

$C(T)/V_0$ approx = 0.179

at T = 26 June 2020, indicating that the majority of the vulnerable pool remains undepleted within the first-wave window.

3.6.3 Waveform similarity despite large mortality differences

A direct comparison between New York and Norway further illustrates the separation between epidemic waveform structure and absolute mortality magnitude (Fig. 10).

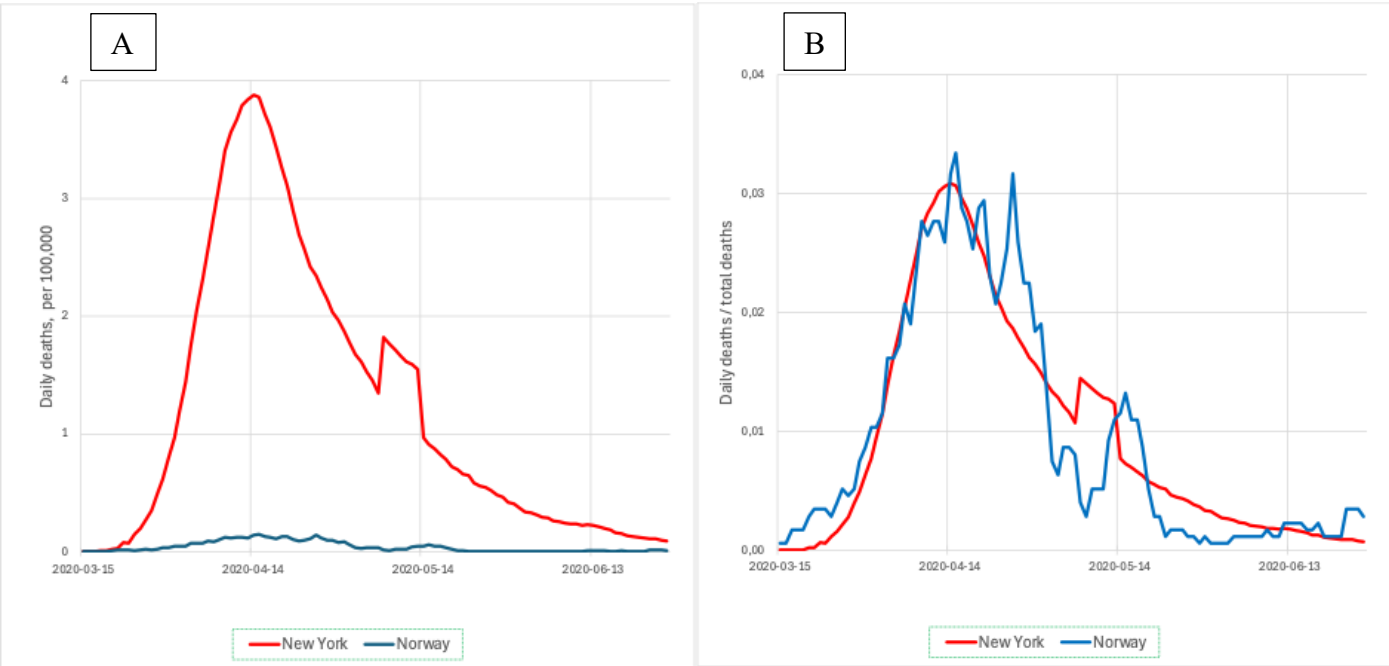

Figure 10. Comparison of epidemic waveforms in New York and Norway.
Panel A: Observed daily mortality per 100,000 population.
Panel B: Normalized daily mortality (daily mortality divided by cumulative mortality at the end of the analysis window).

Despite large differences in absolute mortality magnitude, the normalized epidemic waveforms display highly similar temporal dynamics.

This observation indicates that similar epidemic waveform structures may arise under comparable activation dynamics even when absolute endpoint magnitudes differ substantially across regions.

3.7 Quantitative fit performance

Goodness-of-fit was evaluated on temporally aligned daily mortality incidence using RMSE, MAE, R^2, and Pearson correlation (r) over a standardized 100-day window defined as the first 100 days following the initial recorded death in each region (Table 1).

Region	p_max	RMSE	MAE	R^2	Pearson_r
Belgium	0.050	0.14	0.09	0.97	0.98
Netherlands	0.045	0.07	0.05	0.95	0.98
Spain	0.050	0.15	0.10	0.94	0.97
UK	0.035	0.05	0.04	0.99	0.99
Michigan	0.040	0.06	0.04	0.98	0.99
New Jersey	0.035	0.24	0.18	0.96	0.98
New York State	0.050	0.23	0.14	0.96	0.98
Alabama	0.002	0.04	0.04	0.59	0.77
Florida	0.002	0.02	0.02	0.88	0.94
Texas	0.002	0.01	0.01	0.86	0.93

Table 1. Quantitative agreement between observed and simulated COVID-19 mortality curves. Goodness-of-fit metrics (RMSE, MAE, R^2) were calculated on aligned daily mortality series over a fixed 100-day analysis window. Metrics reflect correspondence in temporal waveform morphology following independent matching of cumulative endpoint magnitude.

Because cumulative endpoint magnitude was matched independently during calibration, the reported metrics primarily quantify correspondence in temporal waveform morphology, including peak timing, amplitude, and decline structure - rather than differences in total mortality burden.

Across European countries and U.S. states, the metrics indicate close structural correspondence between simulated and observed daily mortality curves under the unified SEVA framework.

4. Discussion

The present study examines whether the large-scale waveform structure observed during the first COVID-19 epidemic wave can be reproduced within a minimal activity-driven depletion framework. The results show that a simple formulation in which a time-varying activity function acts on a finite vulnerable population is sufficient to generate the characteristic asymmetric rise–peak–decline patterns observed in hospitalization and mortality data across multiple regions.

In the SEVA framework, epidemic incidence arises from the interaction between a temporally structured activity function A(t) and depletion of the vulnerable pool V(t). As activity increases over time, incidence initially rises; as the vulnerable population becomes progressively depleted, incidence subsequently declines. The epidemic turning point occurs when the increase in activity is balanced by depletion of the remaining vulnerable population. This mechanism produces asymmetric epidemic waves without requiring explicit modelling of infection transmission dynamics or infection-to-event delay distributions.

The model further illustrates that distinct epidemic waveform regimes may arise under different activity intensities. Higher activity intensity produces rapid depletion of the vulnerable population and results in sharply peaked epidemic waves with sustained post-peak decline. In contrast, lower activity intensity leads to incomplete depletion within the observation window, producing plateau-like incidence trajectories. These

two dynamical regimes correspond closely to contrasting epidemic patterns observed during the first COVID-19 wave, including sharply peaked epidemics in several northern regions and more prolonged plateau-like dynamics observed elsewhere.

An important empirical observation emerging from the present analysis is the marked similarity of normalized epidemic waveforms across regions with very different absolute mortality burdens. When cumulative mortality and daily incidence are expressed relative to the final epidemic size, curves from geographically and demographically distinct regions display closely similar temporal structures. This behaviour follows directly from the mathematical structure of the SEVA formulation, in which the normalized epidemic trajectory depends primarily on the time-integrated activity function rather than on the absolute size of the vulnerable population. If the temporal structure of viral activity is broadly similar across regions, normalized epidemic waveforms will therefore tend to converge toward similar shapes.

Mathematically, the SEVA formulation is closely related to hazard-based models widely used in survival analysis. In this interpretation the activity function A(t) represents a time-varying population hazard acting on the remaining vulnerable fraction of the population. Epidemic incidence can therefore be interpreted as the product of exposure intensity and the remaining population capable of contributing to observable endpoints, while the cumulative epidemic trajectory reflects the integrated activity acting on the vulnerable population over time.

Epidemic curves during the first COVID-19 wave have frequently been described as approximately Gompertz-like. In transmission-based epidemic models such behaviour has often been interpreted as evidence of strong heterogeneity in transmission or superspreading dynamics. However, Gompertz trajectories can also be expressed in a hazard–depletion formulation mathematically similar to the SEVA model. In this representation epidemic incidence is proportional to a time-varying hazard acting on the remaining susceptible population. The present results therefore illustrate that Gompertz-like epidemic waveforms do not uniquely imply transmission-driven dynamics, but may also emerge from activity-driven hazard processes.

Within the SEVA framework the activity function should be interpreted as an aggregate representation of temporally structured viral exposure rather than as a directly measurable environmental variable. Several biological processes may contribute to such structured activity. Environmental conditions such as temperature, humidity, and ultraviolet radiation influence viral persistence outside the host, while seasonal variation in host susceptibility and mucosal immunity may modulate effective exposure intensity at the population level. Behavioural synchronization in human populations may further influence patterns of exposure.

When the model is applied at the level of large populations such as countries or states, the activity function should therefore be interpreted as a population-level average of highly heterogeneous local exposure processes. Viral exposure varies substantially across individuals and locations, for example when susceptible individuals come into close proximity with infected persons, where the local viral load in the surrounding environment may be substantially elevated. In this sense, the SEVA formulation does not assume homogeneous exposure but instead describes the average effect of strongly heterogeneous exposure conditions acting on the population as a whole.

More generally, sigmoidal activation followed by a period of sustained activity is a common feature of many biological systems. Comparable activation dynamics are observed in processes such as seasonal pollen release, fungal spore dispersal, and other environmentally modulated biological exposure processes. In this sense the activity function used here should be viewed as a generic dynamical representation of temporally structured biological activation rather than as a claim about a single identifiable environmental mechanism. One possible interpretation is that the activity function reflects access to a broader environmental reservoir of viral material within the biosphere, although the present model does not identify or quantify such a reservoir.

The present study does not attempt to identify the specific biological origin of the activity function, nor does it attempt to reconstruct infection incidence or estimate epidemiological parameters such as reproduction numbers. Instead, the objective is to examine whether the large-scale temporal structure of epidemic waves can be reproduced by a minimal dynamical formulation operating directly at the level of observable endpoints.

Several limitations of this structural approach should therefore be acknowledged. First, the model operates at the level of hospitalization and mortality rather than explicitly modelling infection incidence, and infection-to-event delay distributions are therefore not represented explicitly. Second, the activity function is introduced phenomenologically and is not derived from independently measured environmental variables. Third, model calibration focuses on reproducing waveform morphology rather than performing formal statistical parameter inference. The purpose of the present analysis is therefore structural comparison between model dynamics and observed epidemic waveforms rather than detailed epidemiological parameter estimation.

Despite these simplifications, the SEVA framework captures several robust features of first-wave epidemic dynamics across multiple countries and U.S. states. The results suggest that temporally structured viral activity interacting with depletion of a finite vulnerable population may represent an additional dynamical component contributing to large-scale epidemic patterns.

The SEVA framework may therefore provide a useful complementary perspective for analysing large-scale epidemic waveform dynamics in situations where infection incidence is not directly observable but reliable endpoint data are available.

Conceptual summary

Taken together, the SEVA framework suggests that large-scale epidemic waveforms may arise from the interaction between temporally structured viral activity and depletion of a finite population capable of contributing to observable endpoints. In this formulation, epidemic incidence reflects the product of exposure intensity and the remaining vulnerable population. As activity increases, incidence rises; as the vulnerable pool becomes progressively depleted, incidence declines, producing the characteristic asymmetric epidemic waveform.

When epidemic trajectories are expressed in normalized form, their temporal structure depends primarily on the activity profile rather than on absolute endpoint magnitude. This provides a possible explanation for the striking similarity of normalized epidemic waveforms observed across regions with very different mortality burdens.

Within the SEVA framework, epidemic waves represent the dynamical response of a vulnerable population to temporally structured viral activity.

In this sense, the SEVA framework can be viewed as a testable hypothesis for the dynamical origin of epidemic waveforms, which may be evaluated using epidemic data from different pathogens and epidemiological settings.

Data availability

The datasets generated and analysed during the current study are available in the Zenodo repository: https://doi.org/10.5281/zenodo.19021158

Declaration of generative AI and AI-assisted technologies in the manuscript preparation process

During the preparation of this work the author used ChatGPT in order to to assist with language editing, grammer refinement, and improvement of sentence clarity. After using this tool, the author reviewed and edited the content as needed and takes full responsibility for the content of the published article.

References

Anderson, R.M., May, R.M., 1991. *Infectious Diseases of Humans: Dynamics and Control*. Oxford University Press, Oxford.

Brookmeyer, R., Gail, M.H., 1988. AIDS epidemiology: a quantitative approach. Oxford University Press, New York.

Dowell, S.F., 2001. Seasonal variation in host susceptibility and cycles of certain infectious diseases. *Emerg. Infect. Dis.* 7, 369–374. https://doi.org/10.3201/eid0703.010301

European Centre for Disease Prevention and Control, 2020. COVID-19 surveillance data. European Centre for Disease Prevention and Control, Stockholm. https://www.ecdc.europa.eu

Keeling, M.J., Rohani, P., 2008. *Modeling Infectious Diseases in Humans and Animals*. Princeton University Press, Princeton.

Kermack, W.O., McKendrick, A.G., 1927. A contribution to the mathematical theory of epidemics. *Proc. R. Soc. Lond. A* 115, 700–721. https://doi.org/10.1098/rspa.1927.0118

Mathieu, E., Ritchie, H., Rodés-Guirao, L., et al., 2020. Coronavirus pandemic (COVID-19). *Our World in Data*. https://ourworldindata.org/coronavirus

Shaman, J., Kohn, M., 2009. Absolute humidity modulates influenza survival, transmission, and seasonality. *Proc. Natl. Acad. Sci. U.S.A.* 106, 3243–3248. https://doi.org/10.1073/pnas.0806852106

Tamerius, J.D., Shaman, J., Alonso, W.J., Bloom-Feshbach, K., Uejio, C.K., Comrie, A., Viboud, C., 2011. Environmental predictors of seasonal influenza epidemics across temperate and tropical climates. *PLoS Pathog.* 7, e1003194. https://doi.org/10.1371/journal.ppat.1003194

The COVID Tracking Project, 2021. COVID Tracking Project data archive. The Atlantic, Boston. https://covidtracking.com